SANDIA REPORT
SAND2014-0842
Unlimited Release
Printed February 2014

Electromagnetic Coupling Into Two Standard Calibration Shields On The Sandia Cable Tester

L. K. Warne, L. I. Basilio, W. L. Langston, Electromagnetic Theory Dept.,
K. C. Chen, Nuclear Safety Assessment Dept.,
H. G. Hudson, M. E. Morris, S. L. Stronach, and W. A. Johnson, Retired,
Sandia National Laboratories, Albuquerque, NM
W. Derr, Derr Enterprises, Albuquerque, NM

Prepared by
Sandia National Laboratories
Albuquerque, New Mexico 87185 and Livermore, California 94550

Sandia National Laboratories is a multi-program laboratory managed and operated by Sandia Corporation, a wholly owned subsidiary of Lockheed Martin Corporation, for the U.S. Department of Energy's National Nuclear Security Administration under contract DE-AC04-94AL85000.

Sandia National Laboratories

Issued by Sandia National Laboratories, operated for the United States Department of Energy by Sandia Corporation.

Printed in the United States of America. This report has been reproduced directly from the best available copy.

Available to DOE and DOE contractors from
U.S. Department of Energy
Office of Scientific and Technical Information
P.O. Box 62
Oak Ridge, TN 37831

Telephone: (865) 576-8401
Facsimile: (865) 576-5728
E-Mail: reports@adonis.osti.gov
Online ordering: http://www.osti.gov/bridge

Available to the public from
U.S. Department of Commerce
National Technical Information Service
5285 Port Royal Rd.
Springfield, VA 22161

Telephone: (800) 553-6847
Facsimile: (703) 605-6900
E-Mail: orders@ntis.fedworld.gov
Online order: http://www.ntis.gov/help/ordermethods.asp?loc=7-4-0#online

SAND2014-0842
Unlimited Release
Printed February 2014

Electromagnetic Coupling Into Two Standard Calibration Shields On The Sandia Cable Tester

L. K. Warne, L. I. Basilio, and W. L. Langston, Electromagnetic Theory Dept.,
K. C. Chen, Nuclear Safety Assessment Dept.
H. G. Hudson, M. E. Morris, S. L. Stronach, and W. A. Johnson, Retired
Sandia National Laboratories
P. O. Box 5800
Albuquerque, NM 87185-1152

W. Derr, Derr Enterprises, Albuquerque, NM

Abstract

This report presents analytic transmission line models for calculating the shielding effectiveness of two common calibration standard cables. The two cables have different canonical aperture types, which produce the same low frequency coupling but different responses at resonance. The dominant damping mechanism is produced by the current probe loads at the ends of the cables, which are characterized through adaptor measurements. The model predictions for the cables are compared with experimental measurements and good agreement between the results is demonstrated. This setup constitutes a nice repeatable geometry that nevertheless exhibits some of the challenges involved in modeling non-radio frequency geometries.

Intentionally Left Blank

Contents

Figures

Intentionally Left Blank

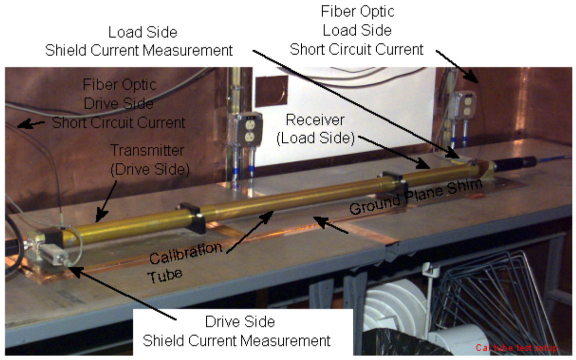

Figure 1. The cable tester arrangement used to measure the shielding effectiveness of the calibration tubes.

Electromagnetic Coupling Into Two Standard Calibration Shields On The Sandia Cable Tester

1 INTRODUCTION

We frequently use a cable tester to measure the shielding effectiveness of multiconductor cables. There are many types of measurement setups for characterizing cable shields [1]. The setup we use is show in Figures 1 (with a blank calibration shield or tube in place of the cable) and 2. The cable above a ground plane arrangement not only mimics actual cable routing, but allows cables of various cross sectional shapes (like flat cables) to be used, including some with branches. Usually the cable pins are tied together in a transition connector at each of the two ends and optically coupled current probes in the tester are used to measure interior and exterior currents. Two calibration standard shields (or tubes), one containing circular holes [2], [3] and the other narrow slots, are used to checkout the tester. This report presents a simple analysis of the setup and a comparison of the predicted and measured results for these calibration tubes. Both the low frequency and resonant limits are examined. The resonance depends on the penetration of the shield construct as well as the current probe terminations, which are interrogated through adaptors. Understanding the performance of the tester with these tubes is important in order to properly interpret its response with actual cables. In addition, this setup constitutes an instructive arrangement since issues arising in the modeling are similar to those arising with actual cables [4] but in a more controlled and repeatable geometry.

2 TRANSMISSION LINE SOURCES

Latham [5] considers field leakage through apertures in an arbitrary cable shield, which we use here. The transfer impedance Z_T and transfer admittance Y_T sources are shown in Figure 3 [6].

2.1 Equivalent Voltage Source

Using time dependence $e^{-i\omega t}$, the equivalent transmission-line voltage source due to a shield aperture

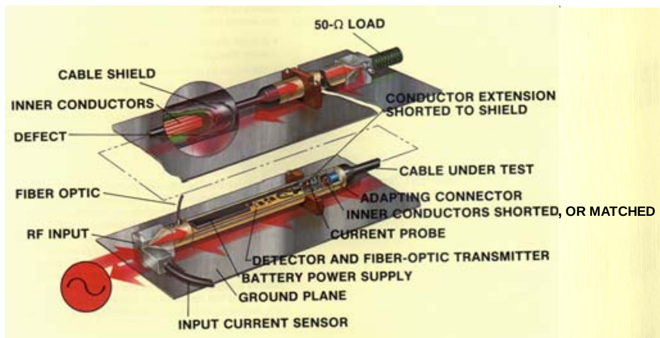

Figure 2. Sketch of cable tester.

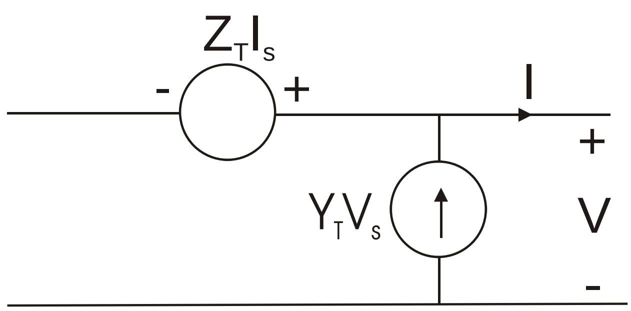

Figure 3. Transfer impedance Z_T and transfer admittance Y_T sources for cable.

A can be rewritten as [5]

$$V_{eq} = -i\omega\mu_0 \int_A \frac{\phi_m^0}{I_0} \frac{\partial \phi_m}{\partial n} dS \tag{1}$$

where the interior magnetic scalar potential ϕ_m^0 is defined as that generated by a current I_0 flowing in the z direction on the center conductor while a z directed return current $-I_0$ flows along the interior of the shield without an aperture (aperture shorted) and the corresponding magnetic field is $\underline{H}_0 = -\nabla\phi_m^0$. The magnetostatic potential ϕ_m corresponds to the difference field $\underline{H} = -\nabla\phi_m$ between the aperture open and closed cases, the unit normal $\underline{n}$ points into the illuminated region from the aperture (away from the coaxial region), and of course since $-\partial\phi_m^0/\partial n$ vanishes in the aperture, $-\partial\phi_m/\partial n$ is equal to the normal magnetic field in the aperture for the open case. The voltage source polarity has a positive reference on the positive z side of the aperture. Letting $\underline{s}$ be a coordinate on the aperture surface and expanding the potential in the center of the aperture $\underline{s} = \underline{s}_A$ as

$$\frac{\phi_m^0}{I_0} \approx \frac{\phi_m^0}{I_0}\left(\underline{s}_A\right) - \underline{H}_0\left(\underline{s}_A\right) \cdot \frac{\underline{s} - \underline{s}_A}{I_0}, \tag{2}$$

the term independent of $\underline{s}$ vanishes and (1) can be rewritten as

$$V_{eq} = -i\omega\mu_0 \frac{1}{2} \underline{f}_I \cdot \underline{m}_a. \tag{3}$$

where the normalized field at the aperture from the coaxial current is

$$\underline{f}_I = \underline{H}_0\left(\underline{s}_A\right) / \left(-I_0\right) = \frac{-1}{2\pi c_i} \underline{e}_\varphi \tag{4}$$

and the final equality is for a circular coaxial arrangement, with inner radius of the shield conductor c_i and azimuthal unit vector $\underline{e}_\varphi$. The magnetic dipole moment of the aperture [6] is defined as

$$\underline{m}_a = -2 \int_A \left(\underline{s} - \underline{s}_A\right) H_n dS. \tag{5}$$

This dipole moment generates the fields on the shadow side of the aperture and includes the ground plane image (so the ground plane is removed when finding the fields from this dipole moment). The normal field in the aperture is approximated by the normal field in the same aperture placed on an infinite ground plane, using the aperture polarizability $\underline{\alpha}_m$ (which only has components in the plane of the aperture) and the short circuit external field at the center of the aperture $\underline{H}_{sc}\left(\underline{s}_A\right)$ [6],

$$\underline{m}_a = -2\underline{\alpha}_m \cdot \underline{H}_{sc}\left(\underline{s}_A\right) \tag{6}$$

The short circuit magnetic field drive of the apertures is obtained by taking into account the variation of the electric current density on the exterior of the cable test fixture. To determine this parameter, a cylinder of outer radius $c_e = c_i + \Delta$ (where Δ represents the thickness of the conductor metal) carrying total current I_s at a height h above a ground plane is considered and replaced by a filament at the image height

$$h_e = \sqrt{h^2 - c_e^2} \tag{7}$$

The short circuit exterior magnetic field for this filament, and its image carrying current $-I_s$ at a location h_e below the ground plane, gives the normalized exterior field at the aperture

$$\underline{f}_E = \underline{H}_{sc} / \left(-I_s\right) = \frac{-1}{2\pi c_e} \frac{h_e}{h + c_e \sin\varphi} \underline{e}_\varphi \tag{8}$$

where φ is the azimuth angle about the cylindrical conductor ($\varphi = \pi/2$ corresponds to the top of the conductor, $\varphi = -\pi/2$ corresponds to the bottom of the conductor, and $\varphi = 0, \pi$ correspond to the sides of the conductor). Note that the integration of the magnetic field around the cylinder must yield the shield current and thus

$$\frac{1}{2\pi}\int_{-\pi}^{\pi} \frac{h_e}{h + c_e \sin\varphi} d\varphi = 1$$

Thus for a large number of apertures around the tube, approaching a continuous distribution in the azimuth, there is no correction due to the asymmetric distribution of current density; a correction only results because of the limited number of apertures. The equivalent voltage source can then be rewritten as

$$V_{eq} = -i\omega I_s \mu_0 \underline{f}_I \cdot \underline{\alpha}_m \cdot \underline{f}_E(\underline{s}_A) = -i\omega I_s \frac{\mu_0 \alpha_m}{(2\pi c_i)(2\pi c_e)} \frac{h_e}{h + c_e \sin\varphi_A} \tag{9}$$

where φ_A is the angle about the cylinder axis corresponding to the center of each particular aperture. Each calibration tube is made up of four apertures around the circumference, with 11 sets of apertures spaced $d = 2$ in. apart along a cylinder. Summing over the four hole positions around the circumference (positioned at $\varphi_A = -\pi/2, 0, \pi/2, \pi$) gives

$$V_{eq} = -i\omega\mu_0 \frac{I_s \alpha_m}{\pi c_i \pi c_e} f_{4E} \tag{10}$$

where the final factor results from the asymmetry of the current density

$$f_{4E} = \frac{h^2 - c_e^2/2}{h h_e}$$

Note that the transfer inductance per unit length is

$$L_T = \mu_0 \frac{\alpha_m}{\pi c_i \pi c_e d} f_{4E}$$

where

$$v_{eq} = V_{eq}/d = Z_T I_s = -i\omega L_T I_s$$

2.2 Equivalent Current Source

Similarly the equivalent transmission-line current source due to a shield aperture A can be rewritten as [5]

$$I_{eq} = i\omega\epsilon_0 C_0 \int_A \frac{1}{Q_0} \frac{\partial\phi^0}{\partial n} \phi dS \tag{11}$$

the electric scalar potential ϕ^0 corresponds to the field $\underline{E}_0 = -\nabla\phi^0$ when the shield is complete (the aperture is shorted) and a charge per unit length Q_0 exists on the center conductor with a charge $-Q_0$ on the interior of the shield (note that we set $\phi^0 = 0$ on the shield and $\phi^0 = Q_0/C_0$ on the center conductor, where C_0 is the interior capacitance per unit length of the transmission line). The potential ϕ corresponds to the difference field $\underline{E} = -\nabla\phi$ between the aperture open and closed cases. The equivalent current source direction is from the shield to the center conductor (current is injected into the center conductor). Using duality

$$\frac{\epsilon_0}{Q_0}\frac{\partial \phi^0}{\partial n} = \left(\underline{e}_z \times \underline{f}_I\right) \cdot \underline{n} \tag{12}$$

where $\underline{e}_z$ is the axial unit vector. If we approximate $\underline{f}_I$ at the center of the aperture we can bring it outside the integral and write

$$I_{eq} = i\omega \left(C_0/\epsilon_0\right) \frac{1}{2} \left[\underline{e}_z \times \underline{f}_I \left(\underline{s}_A\right)\right] \cdot \underline{p}_a \tag{13}$$

where the electric dipole moment is [6]

$$\underline{p}_a = -2\epsilon_0 \underline{n} \int_A \phi dS \tag{14}$$

As in the magnetostatic analysis in the previous section, this dipole moment generates the fields on the shadow side of the aperture and includes the ground plane image (so the ground plane is removed when finding the fields from this dipole moment). Again the potential in the aperture is approximated by the potential in the same aperture placed on an infinite ground plane. In this case, the electric dipole moment can be written in terms of the polarizability $\underline{\alpha}_e$ and the short circuit external field at the center of the aperture $\underline{E}_{sc}\left(\underline{s}_A\right)$

$$\underline{p}_a = 2\epsilon_0 \underline{\alpha}_e \cdot \underline{E}_{sc}\left(\underline{s}_A\right) \tag{15}$$

and the tensor polarizability $\underline{\alpha}_e$ only has a component normal to the plane.

The variation of the electric charge density on the exterior of the test fixture gives the short circuit electric field drive of the apertures

$$\underline{E}_{sc}\epsilon_0/Q_s = \underline{e}_z \times \underline{f}_E \tag{16}$$

where Q_s is the exterior charge per unit length on the shield and the equivalent current source can then be written as

$$I_{eq} = i\omega Q_s \left(C_0/\epsilon_0\right) \left[\underline{e}_z \times \underline{f}_I \left(\underline{s}_A\right)\right] \cdot \underline{\alpha}_e \cdot \left[\underline{e}_z \times \underline{f}_E \left(\underline{s}_A\right)\right] = i\omega Q_s \left(C_0/\epsilon_0\right) \frac{\alpha_e}{4\pi^2 c_i c_e} \frac{h_e}{h + c_e \sin\varphi_A} \tag{17}$$

Relating the charge per unit length to the exterior voltage, and for a traveling wave to the current,

$$Q_s = CV_s = CZ_cI_s = I_s/c \tag{18}$$

where C is the capacitance per unit length of the exterior with respect to the ground plane, V_s is the voltage of the exterior with respect to the ground plane, and $Z_c = \sqrt{L/C}$ is the characteristic impedance between the exterior conductor and the ground plane. The characteristic impedance is written in terms of the per unit length inductance and capacitance of the exterior region (L and C, respectively, where $\sqrt{LC} = 1/c$ and c is the velocity of light). Note that the continuity equation yields

$$\frac{dI_s}{dz} = i\omega Q_s \tag{19}$$

and for a forward propagating wave (matched exterior transmission line) $dI_s/dz = ikI_s$ where $k = \omega\sqrt{LC}$. Summing over the 4 holes around the circumference gives

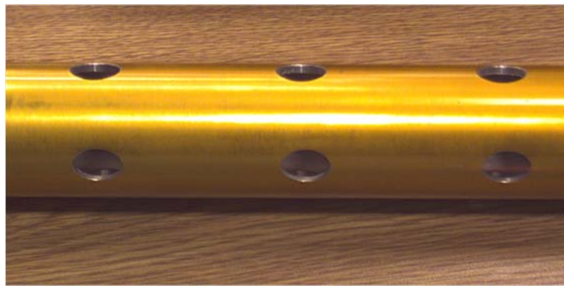

Figure 4. Cylindrical shield with periodic set of four circumferential circular apertures.

$$I_{eq} = i\omega Q_s \left(C_0/\epsilon_0\right) \frac{\alpha_e}{\pi c_i \pi c_e} f_{4E} = ikI_s \left(C_0/\epsilon_0\right) \frac{\alpha_e}{\pi c_i \pi c_e} f_{4E} \tag{20}$$

where the final equality holds for a traveling wave exterior current. Note that the transfer capacitance per unit length is

$$C_T = -\left(CC_0/\epsilon_0\right) \frac{\alpha_e}{\pi c_i \pi c_e d} f_{4E}$$

where

$$i_{eq} = I_{eq}/d = Y_T V_s = -i\omega C_T V_s$$

2.3 Polarizabilities

The polarizabilities for both tubes are now given.

2.3.1 Circular Aperture Tube

Figure 4 shows the tube with circular holes. For radius a in a zero thickness planar screen the polarizabilities are [6]

$$\alpha_m^0 = \frac{4}{3} a^3 \tag{21}$$

$$\alpha_e^0 = \frac{2}{3} a^3 \tag{22}$$

where in the planar equivalent (of the cylindrical system) $\alpha_m = \alpha_{mxx} = \alpha_{mzz}$, $\alpha_e = \alpha_{eyy}$.The shield in this case has a wall thickness of $\Delta \approx 0.116$ in., with a circular hole diameter of $2a \approx 0.486$ in.. Thus, for this case, a wall-thickness correction is applied by recognizing from [7] and [8] that with $\Delta/a \approx 0.477$, the error in using the $\Delta/a \to \infty$ asymptotic formula versus the numerical solution is limited to approximately 1% in the magnetic polarizability and 2% in the electric polarizability. Therefore we have

$$\alpha_m \approx \alpha_m^0 \, 0.838 \, e^{-j'_{11}(\Delta/a)} \approx 1.09102 \times 10^{-7} \text{ m}^3 \tag{23}$$

where $j'_{11} = 1.841$ is the first root of $J'_1(x) = 0$, and

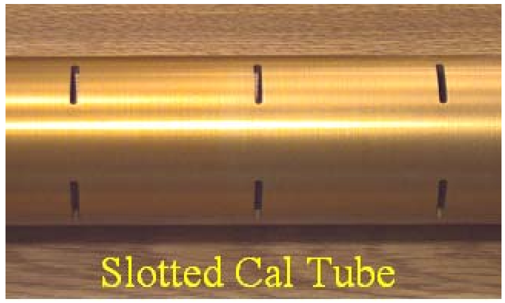

Figure 5. Cylindrical shield with a periodic set of four circumferential rectangular-slot apertures.

$$\alpha_e \approx \alpha_e^0 \, 0.825 e^{-j_{0,1}(\Delta/a)} \approx 0.410283 \times 10^{-7} \text{ m}^3 \tag{24}$$

[8] where $j_{0,1} = 2.405$ is the first root of $J_0(x) = 0$.

2.3.2 Slot Aperture Tube

Figure 5 shows the slotted calibration shield. The dominant length directed magnetic polarizability for a narrow slot of length ℓ_s and width w with $\ell_s >> w$ is given by [9]

$$\alpha_m = \alpha_{mxx} \sim \frac{\pi \ell_s^3}{12\Omega_e} \tag{25}$$

where the parameter Ω_e is

$$\Omega_e = 2\left[\ln(2\ell_s/a_e) - 7/3\right] \tag{26}$$

and the much smaller electric (as well as the other component of the magnetic) polarizability is

$$\alpha_e \sim \pi a_e^2 \ell_s \sim \alpha_{mzz} \approx 0.0023929 \times 10^{-7} \text{ m}^3 \tag{27}$$

where the equivalent radius is given by

$$a_e = w/4 \tag{28}$$

The dimensions here are $w \approx 0.09$ in., $\ell_s \approx 0.6$ in, and $\Delta \approx 0.116$ in. For the case where the thickness is much smaller than the slot length $\Delta << \ell_s$, the wall thickness is accounted for in this case by simply rewriting the equivalent radius as [9]

$$a_e \approx \frac{w}{4} e^{-\pi\Delta/(2w)} \tag{29}$$

or for $\Delta >> w$

$$a_e \sim \frac{2w}{\pi e} e^{-\pi\Delta/(2w)} \; , \; \Delta/w >> 1 \tag{30}$$

This second asymptotic form is quite accurate for $\Delta/w \geq 0.25$. The thickness results in an even smaller equivalent radius and thus makes the electric polarizability negligible.

The axial polarizability for a slot with unrestricted wall thickness is given in [10] as

$$\alpha_{mxx} \approx \frac{16\ell_s^4/\left(\pi^3 w\right)}{\left[\Omega_e^0 \sinh\left(\frac{\pi\Delta}{2\ell_s}\right) + (2\ell_s/w)\cosh\left(\frac{\pi\Delta}{2\ell_s}\right)\right]\left[\Omega_e^0 \cosh\left(\frac{\pi\Delta}{2\ell_s}\right) + (2\ell_s/w)\sinh\left(\frac{\pi\Delta}{2\ell_s}\right)\right]} \tag{31}$$

$$\approx 1.07751 \times 10^{-7}\ \mathrm{m}^3$$

where

$$\Omega_e^0 = 2\left[\ln\left(8\ell_s/w\right) - 7/3\right] \tag{32}$$

3 SHIELDING EFFECTIVENESS

We now give the shielding effectiveness defined as the ratio of interior to exterior currents on the tubes.

3.1 LOW FREQUENCY SOLUTION

The exterior characteristic impedance for a cylinder of radius c_e at a height h above a ground plane is

$$Z_c = \frac{\eta_0}{2\pi}\mathrm{Arccosh}\left(h/c_e\right) \tag{33}$$

where $\eta_0 = \sqrt{\mu_0/\epsilon_0} \approx 120\pi$ ohms is the impedance of free space. Assuming $Z_c = 50$ ohms and $c_e = 0.9375$ in., the height is found to be $h \approx 1.2823$ in. Thus, for this case, the factor in (10) and (20) which accounts for nonuniformity of the exterior current density due to the proximity of the ground plane

$$f_{4E} \approx 1.074$$

is found to be close to unity [2]. The internal inductance of the coaxial region of length $\ell \approx 26$ in. (formed by the calibration tube and an inner conductor of radius $b \approx 0.125$ in.) is approximately

$$L_{tot} = \ell L_0 = \ell\frac{\mu_0}{2\pi}\ln\left(c_i/b\right) \approx 0.2487\mu\mathrm{H} \tag{34}$$

(the small correction resulting from the apertures has been ignored). The low frequency interior current at the ends of the transmission line (with short circuit loads) is thus given by

$$I = I_s \ell_{eq} L_T / L_{tot} = I_s \frac{\ell_{eq} L_T}{\ell L_0} \tag{35}$$

where the shielding effectiveness of the calibration tube is then

$$I/I_s \sim 11\alpha_m \frac{\mu_0/L_{tot}}{\pi^2 c_i c_e} f_{4E} \tag{36}$$

Here the factor of 11 arises from the eleven sets of holes along the tube axis. Evaluating this for the cable parameters given above, the low-frequency shielding effectiveness for the circular-hole calibration standard is

$$I/I_s \approx 0.00133\left(-57.5\ \mathrm{dB}\right) \tag{37}$$

which by design is nearly the same value for the slotted calibration standard.

At each end of the tester there are 50 ohm current measurement systems with 10 to 1 transformers. Thus one half ohm loads are present

$$Z_L = R_L = 50 \text{ ohm}/10^2 = 0.5 \text{ ohm}$$

We expect the frequency for which these compete with the inductive reactance to be down around

$$\omega_L = 2R_L/L_{tot}$$

or 320 kHz.

3.2 General Solution

The general solution is now found for an exterior traveling wave current

$$I_s = I_{s0}e^{ikz}$$

Near the first resonance the end current probe loads represent the dominant loss mechanism in the line. In this section the axial spacing between sets of holes d is assumed to be small compared to the wavelength so we can take the sources to be continuously distributed over a distance of

$$\ell_{eq} = 11d = 22 \text{ in}$$

with a spacing of 2 in from each of the two loads (the last aperture is actually 3 in from each load). The distributed voltage and current source strengths over the driven region $|z| < \ell_{eq}/2$ are

$$v_{eq} = v_{s0}e^{ikz} \tag{38}$$

$$i_{eq} = i_{s0}e^{ikz} \tag{39}$$

where V_{eq} is given by (10), and I_{eq} is given by (20) and v_{s0} and i_{s0} are constant amplitudes. The transmission line equations for the interior are

$$\frac{dV}{dz} = i\omega L_0 I + v_{eq} \tag{40}$$

$$\frac{dI}{dz} = i\omega C_0 V + i_{eq} \tag{41}$$

These equations are used for $|z| < \ell_{eq}/2$ but can also be applied outside the source region by taking the drives v_{eq} and i_{eq} to vanish for $\ell_{eq}/2 < |z| < \ell/2$. Eliminating the voltage from the transmission line equations gives

$$\left(\frac{d^2}{dz^2} + k^2\right) I = \frac{di_{eq}}{dz} + i\omega C_0 v_{eq} = A_{eq}e^{ikz} \text{ , } |z| < \ell_{eq}/2 \tag{42}$$

Here $\omega\sqrt{L_0C_0} = k_0 = k$ (since dielectric materials around the conductors are not being considered) is the wavenumber for the interior region and

$$A_{eq} = i\left(ki_{s0} + \omega C_0 v_{s0}\right) = k^2 I_{s0}\left[\left(C_T/C\right) + \left(C_0/\varepsilon_0\right)\left(L_T/\mu_0\right)\right] = \left(C_0/\epsilon_0\right) I_{s0}\left(\alpha_m - \alpha_e\right)\frac{k^2}{\pi^2 c_i c_e d} f_{4E} \qquad (43)$$

It is convenient to break the right hand side of (42) into even and odd parts since the geometry is symmetric along its length (in z with the origin taken at the center of the line). Thus, the interior transmission line current can be written as

$$I = I_{even} + I_{odd}$$

where

$$I_{even} = A_{even}\cos kz + \frac{1}{2k}A_{eq} z \sin kz \qquad (44)$$

$$I_{odd} = A_{odd}\sin kz - \frac{i}{2k}A_{eq} z \cos kz \qquad (45)$$

and A_{even} and A_{odd} are arbitrary coefficients. The load $Z_L = R_L - iX_L$ terminates the line at $z = \pm\ell/2$ but can be transformed to $\pm\ell_{eq}/2$ as Z_L', where [11]

$$\pm\frac{V\left(\pm\ell_{eq}/2\right)}{I\left(\pm\ell_{eq}/2\right)} = Z_L' = Z_0\left[\frac{Z_L\cos\frac{k}{2}\left(\ell-\ell_{eq}\right) - iZ_0\sin\frac{k}{2}\left(\ell-\ell_{eq}\right)}{Z_0\cos\frac{k}{2}\left(\ell-\ell_{eq}\right) - iZ_L\sin\frac{k}{2}\left(\ell-\ell_{eq}\right)}\right] \approx Z_L - iZ_0 k\left(\ell-\ell_{eq}\right)/2 \qquad (46)$$

and

$$Z_0 = \sqrt{L_0/C_0} = \frac{\eta_0}{2\pi}\ln\left(c_i/b\right) \approx 113 \text{ ohms}$$

is the characteristic impedance of the coaxial region; the final approximation follows because $\left(\ell-\ell_{eq}\right)/2 \approx 2$ in. is short compared to the wavelength and because $Z_L/Z_0 << 1$. The boundary condition (46) can be written as

$$\frac{dI}{dz}\left(\pm\ell_{eq}/2\right) - i_{eq}\left(\pm\ell_{eq}/2\right) = \pm i\omega C_0 Z_L' I\left(\pm\ell_{eq}/2\right) \qquad (47)$$

or

$$\frac{dI_{even}}{dz}\left(\ell_{eq}/2\right) - i\omega C_0 Z_L' I_{even}\left(\ell_{eq}/2\right) = i_{s0} i \sin\left(k\ell_{eq}/2\right) \qquad (48)$$

and

$$\frac{dI_{odd}}{dz}\left(\ell_{eq}/2\right) - i\omega C_0 Z_L' I_{odd}\left(\ell_{eq}/2\right) = i_{s0}\cos\left(k\ell_{eq}/2\right) \qquad (49)$$

Substituting (44) and (45) into these boundary conditions, the arbitrary coefficients A_{even} and A_{odd} are found from

$$-kA_{even}\sin\left(k\ell_{eq}/2\right) + \frac{1}{2k}A_{eq}\left\{\sin\left(k\ell_{eq}/2\right) + \left(k\ell_{eq}/2\right)\cos\left(k\ell_{eq}/2\right)\right\}$$

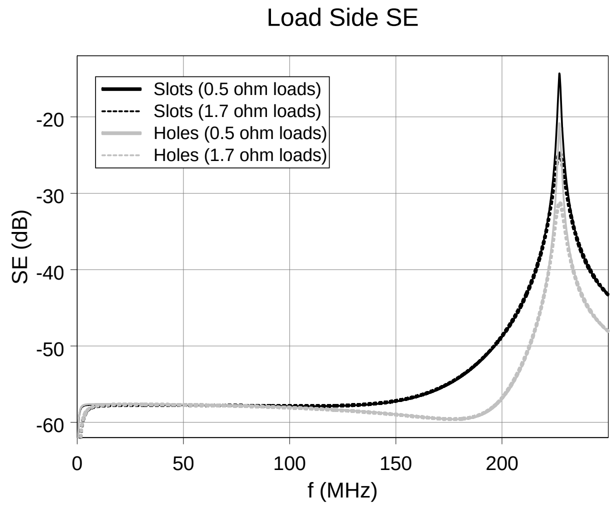

Figure 6. Calculated shielding effectiveness for both slotted and circular hole calibration tubes with 0.5 ohm and 1.7 ohm loads.

$$-i\omega C_0 Z_L' \left[A_{even}\cos\left(k\ell_{eq}/2\right) + \frac{1}{2k}A_{eq}\left(\ell_{eq}/2\right)\sin\left(k\ell_{eq}/2\right)\right] = i_{s0} i \sin\left(k\ell_{eq}/2\right) \tag{50}$$

$$kA_{odd}\cos\left(k\ell_{eq}/2\right) - \frac{i}{2k}A_{eq}\left\{\cos\left(k\ell_{eq}/2\right) - \left(k\ell_{eq}/2\right)\sin\left(k\ell_{eq}/2\right)\right\}$$

$$-i\omega C_0 Z_L' \left[A_{odd}\sin\left(k\ell_{eq}/2\right) - \frac{i}{2k}A_{eq}\left(\ell_{eq}/2\right)\cos\left(k\ell_{eq}/2\right)\right] = i_{s0}\cos\left(k\ell_{eq}/2\right) \tag{51}$$

The total interior current I at each end of the transmission line is hence given by

$$I\left(\pm\ell/2\right) = I\left(\pm\ell_{eq}/2\right)\left[\cos\frac{k}{2}\left(\ell - \ell_{eq}\right) + i\left(Z_L'/Z_0\right)\sin\frac{k}{2}\left(\ell - \ell_{eq}\right)\right] \tag{52}$$

Figure 6 shows the slotted as well as the circular calibration tube response for two assumed real loads. The 0.5 ohm value is the low frequency limit discussed above; the 1.7 ohm value was used because it fits the peak height in the experiment. Notice that the change in load value only has an impact on the peak height and the very low frequency region. This is the expected effect from the preceding inductive solution, where the small load value did not come into the solution, except at the very low frequencies. We also see that the calibration tube with circular holes has reduced penetration compared to the slotted tube. This is also expected from the cancellation of the magnetic and electric polarizability contributions near resonance as discussed in the next subsection.

3.3 First Resonance

Due to the complicated nature of the preceding exact expressions for the current it is useful to find a simpler form near the frequency of the first resonance. Near the first resonance the interior current takes the form

$$I \sim A_1 \sin kz \approx A_1 \sin\left(\frac{\pi}{\ell}z\right) = A_1 \cos\frac{\pi}{\ell}\left(z - \ell/2\right) \tag{53}$$

where the final approximate equality holds because of the low impedance of the loads $Z_L << Z_0$ at $z = \pm\ell/2$. Taking the current to be expanded in a set of orthogonal modes

$$I = \sum_{n=0}^{\infty} A_n \cos\frac{n\pi}{\ell}\left(z - \ell/2\right) \tag{54}$$

such that $V\left(\pm\ell/2\right) \to 0$, then the amplitude can be found by the use of the orthogonality relation

$$\int_{-\ell/2}^{\ell/2} \cos\frac{n\pi}{\ell}\left(z - \ell/2\right)\cos\frac{n'\pi}{\ell}\left(z - \ell/2\right)dz = \ell\delta_{nn'}/\epsilon_n \tag{55}$$

where $\epsilon_n = 1$ for $n = 0$ and $\epsilon_n = 2$ for $n \geq 1$. Thus from (42) (extended to $\pm\ell/2$ by the inclusion of delta and unit step functions)

$$\left(\frac{d^2}{dz^2} + k^2\right)I = \frac{di_{eq}}{dz} + i\omega C_0 v_{eq}$$

$$= A_{eq}e^{ikz}\left[u\left(z + \ell_{eq}/2\right) - u\left(z - \ell_{eq}/2\right)\right] +$$

$$i_{s0}e^{ikz}\left[\delta\left(z + \ell_{eq}/2\right) - \delta\left(z - \ell_{eq}/2\right)\right]\ , 3pt\, |z| < \ell/2 \tag{56}$$

the modal coefficients are found using

$$\frac{\ell}{\epsilon_n}\left[k^2 - \left(\frac{n\pi}{\ell}\right)^2\right]A_n = A_{eq}\int_{-\ell_{eq}/2}^{\ell_{eq}/2} \cos\frac{n\pi}{\ell}\left(z - \ell/2\right)e^{ikz}dz$$

$$+i_{s0}\left[\cos\frac{n\pi}{2\ell}\left(\ell + \ell_{eq}\right)e^{-ik\ell_{eq}/2} - \cos\frac{n\pi}{2\ell}\left(\ell - \ell_{eq}\right)e^{ik\ell_{eq}/2}\right] \tag{57}$$

The first resonant mode thus has amplitude given by

$$\frac{\ell}{2}\left[k^2 - \left(\frac{\pi}{\ell}\right)^2\right]A_1 = i2A_{eq}\int_0^{\ell_{eq}/2} \sin\left(\frac{\pi}{\ell}z\right)\sin\left(kz\right)dz - i_{s0}2\sin\left(\frac{\pi\ell_{eq}}{2\ell}\right)\cos\left(k\ell_{eq}/2\right) \tag{58}$$

where, by introducing the quality factor for the first mode Q_1, this becomes

$$\frac{\ell}{2}\left[k^2 - \left(\frac{\pi}{\ell}\right)^2\left(1 - \frac{i}{2Q_1}\right)^2\right]A_1 \approx i2A_{eq}\int_0^{\ell_{eq}/2} \sin^2\left(\frac{\pi}{\ell}z\right)dz - i_{s0}2\sin\left(\frac{\pi\ell_{eq}}{2\ell}\right)\cos\left(\frac{\pi\ell_{eq}}{2\ell}\right)$$

$$= iA_{eq}\ell_{eq}/2\left[1 - \frac{\ell}{\ell_{eq}\pi}\sin\left(\frac{\pi}{\ell}\ell_{eq}\right)\right] - i_{s0}\sin\left(\frac{\pi\ell_{eq}}{\ell}\right) \tag{59}$$

or

$$\left[k^2 - \left(\frac{\pi}{\ell}\right)^2\left(1 - \frac{i}{2Q_1}\right)^2\right]A_1 \approx iA_{eq}^{-}\ell_{eq}/\ell - iA_{eq}^{+}\frac{1}{\pi}\sin\left(\pi\ell_{eq}/\ell\right) \tag{60}$$

Here

$$A_{eq}^{\pm} = (\eta_0/Z_0)\, I_{s0} \frac{\alpha_m \pm \alpha_e}{\ell^2 c_i c_e d} f_{4E} \tag{61}$$

where Z_0 is again the characteristic impedance of the coaxial region and the quality factor Q_1 can be evaluated by means of

$$Q_1 = \frac{\omega W}{P} \tag{62}$$

where the average power loss (resulting from the end loads alone) is

$$P = \frac{1}{2} R_L \left| I\left(-\ell/2\right) \right|^2 + \frac{1}{2} R_L \left| I\left(\ell/2\right) \right|^2 \approx R_L \left| A_1 \right|^2 \tag{63}$$

and the energy stored is

$$W = \frac{1}{2} L_0 \int_{-\ell/2}^{\ell/2} \left| I(z) \right|^2 dz \approx L_0 \left| A_1 \right|^2 \int_0^{\ell/2} \sin^2\left(\frac{\pi}{\ell} z\right) dz = \frac{\ell}{4} L_0 \left| A_1 \right|^2 \tag{64}$$

If it were desired to add the power lost on the rod, due to conductor surface resistance $R_s = \sqrt{\omega\mu/\left(2\sigma\right)}$, it is

$$P_{abs} = \frac{1}{2} \frac{R_s}{2\pi b} \int_{-\ell/2}^{\ell/2} \left| I(z) \right|^2 dz = \frac{R_s}{2\pi b} \left| A_1 \right|^2 \int_0^{\ell/2} \sin^2\left(\frac{\pi}{\ell} z\right) dz = \frac{R_s}{2\pi b} \frac{\ell}{4} \left| A_1 \right|^2$$

Furthermore, if it is desired to capture the frequency shift resulting from the load reactance X_L we can write the complex power as

$$P = \frac{1}{2} Z_L \left| I\left(-\ell/2\right) \right|^2 + \frac{1}{2} Z_L \left| I\left(\ell/2\right) \right|^2 \approx Z_L \left| A_1 \right|^2$$

Using this to define a complex value of Q_1 through $1/Q_1^c = P/\left(\omega W\right) = 1/Q_1 - iX_L/\left(\omega \ell L_0/4\right)$ we see that this defines a new shifted form

$$\left[k^2 - \left(\frac{\pi}{\ell}\right)^2 \left(1 - \frac{i}{2Q_1} - \frac{X_L}{\omega \ell L_0/2}\right)^2 \right] A_1 \approx i A_{eq}^{-} \ell_{eq}/\ell - i A_{eq}^{+} \frac{1}{\pi} \sin\left(\pi \ell_{eq}/\ell\right) \tag{65}$$

Noting that $k = \pi/\ell$ corresponds to a resonant frequency of 227 MHz, we can put this initial value for ω_0 into the new X_L perturbation term and recompute the resonance condition as $k \approx \left(\pi/\ell\right)\left[1 - X_L/\left(\omega_0 \ell L_0/2\right)\right]$; for a value $X_L \approx 15$ ohms we find the corresponding resonance to be 208 MHz.

The first resonant quality factor (assuming 0.5 ohm loads) is

$$Q_1 \approx \frac{\omega \ell L_0}{4R_L} \approx 177.3 \tag{66}$$

and for 1.7 ohm loads

$$Q_1 \approx 52.2$$

The peak value of the current is

$$A_1 \approx Q_1 \left(\frac{\ell}{\pi}\right)^2 \left[A_{eq}^{-} \ell_{eq}/\ell - A_{eq}^{+} \frac{1}{\pi} \sin\left(\pi \ell_{eq}/\ell\right) \right] \approx Q_1 \left(\frac{\ell}{\pi}\right)^2 \left[A_{eq}^{-} \ell_{eq}/\ell - A_{eq}^{+} \left(1 - \ell_{eq}/\ell\right) \right]$$

$$= I_{s0}Q_1\left(\eta_0/Z_0\right)\frac{\alpha_m\left\{\ell_{eq}/\ell - \frac{1}{\pi}\sin\left(\pi\ell_{eq}/\ell\right)\right\} - \alpha_e\left\{\ell_{eq}/\ell + \frac{1}{\pi}\sin\left(\pi\ell_{eq}/\ell\right)\right\}}{\pi^2 c_i c_e d} f_{4E}$$

$$\approx I_{s0}Q_1\left(\eta_0/Z_0\right)\frac{\alpha_m\left(2\ell_{eq}/\ell - 1\right) - \alpha_e}{\pi^2 c_i c_e d} f_{4E} \tag{67}$$

For the 0.5 ohm load with circular holes the shielding effectiveness at the first resonance becomes

$$A_1/I_{s0} \approx -21.1 \text{ dB} \tag{68}$$

whereas for the 1.7 ohm load with circular holes

$$A_1/I_{s0} \approx -31.7 \text{ dB}$$

For the slotted tube with 0.5 ohm loads

$$A_1/I_{s0} \approx -14.4 \text{ dB} \tag{69}$$

and with 1.7 ohm loads

$$A_1/I_{s0} \approx -25.0 \text{ dB}$$

Figure 6 in the preceding subsection is consistent with these peak values. The fact that the slotted tube has a considerably larger response even though the magnetic polarizabilities of the two tubes are nearly the same results from the cancellation of the magnetic and electric drives near resonance in the circular hole case (as can be seen in the preceding formula), whereas for the slotted tube the electric drive is near zero. This interesting change in response is an analog of other types of cancellation that occur in actual braided cables.

3.3.1 Discrete Aperture Placement At Resonance

To be certain that the error introduced by the approximate continuous distribution of sources, versus the actual discrete set, is not large (an axial equivalent to the preceding finite set used in the azimuth), this section will use the sum of the actual discrete aperture locations to predict the shielding effectiveness. The transmission line equations for a single set of four apertures at $z = z'$ are

$$\frac{dV}{dz} = i\omega L_0 I + V_{eq}\delta\left(z - z'\right) \tag{70}$$

and

$$\frac{dI}{dz} = i\omega C_0 V + I_{eq}\delta\left(z - z'\right) \tag{71}$$

Eliminating V gives

$$\left(\frac{d^2}{dz^2} + k^2\right) I = \frac{d}{dz}\left\{I_{eq}\delta\left(z - z'\right)\right\} + i\omega C_0 V_{eq}\delta\left(z - z'\right) \tag{72}$$

where taking I to be representable as the set of modes (54) over m from $m = -5$ to $+5$ (with $z' = md$) and using the orthogonality relation in (55),

$$\frac{\ell}{\epsilon_n}\left[k^2-\left(\frac{n\pi}{\ell}\right)^2\right]A_n = d\sum_{m=-5}^{5} e^{ikmd}\left[i_{s0}\left(\frac{n\pi}{\ell}\right)\sin\frac{n\pi}{\ell}\left(md-\ell/2\right)+i\omega C_0 v_{s0}\cos\frac{n\pi}{\ell}\left(md-\ell/2\right)\right] \tag{73}$$

Inserting the finite quality factor for the first mode $n=1$ thus gives

$$\frac{\ell}{2}\left[k^2-\left(\frac{\pi}{\ell}\right)^2\left(1-\frac{i}{2Q_1}\right)^2\right]A_1$$

$$\approx -d\sum_{m=-5}^{5}\left[i_{s0}\left(\frac{\pi}{\ell}\right)\cos\left(kmd\right)\cos\left(m\pi d/\ell\right)+\omega C_0 v_{s0}\sin\left(kmd\right)\sin\left(m\pi d/\ell\right)\right] \tag{74}$$

Replacing k by the resonant value π/ℓ on the right hand side, and using identities $2\sin^2 x = 1-\cos\left(2x\right)$ and $2\cos^2 x = 1+\cos\left(2x\right)$, gives

$$\left[k^2-\left(\frac{\pi}{\ell}\right)^2\left(1-\frac{i}{2Q_1}\right)^2\right]A_1$$

$$\approx -\frac{d}{\ell}\sum_{m=-5}^{5}\left[\left(\omega C_0 v_{s0}+i_{s0}\pi/\ell\right)-\left(\omega C_0 v_{s0}-i_{s0}\pi/\ell\right)\cos\left(2m\pi d/\ell\right)\right]$$

$$= i11\frac{d}{\ell}A_{eq}^{-}-i\frac{d}{\ell}A_{eq}^{+}\left[1+\sum_{m=1}^{5}\left(e^{i2m\pi d/\ell}+e^{-i2m\pi d/\ell}\right)\right] \tag{75}$$

Using the geometrical series formula $\sum_{m=1}^{M} r^m = r\left(1-r^M\right)/\left(1-r\right)$ this can be written as

$$\left[k^2-\left(\frac{\pi}{\ell}\right)^2\left(1-\frac{i}{2Q_1}\right)^2\right]A_1$$

$$\approx i11\frac{d}{\ell}A_{eq}^{-}-i\frac{d}{\ell}A_{eq}^{+}\frac{\sin\left(11\pi d/\ell\right)}{\sin\left(\pi d/\ell\right)} = iA_{eq}^{-}\ell_{eq}/\ell - iA_{eq}^{+}\frac{\sin\left(\pi\ell_{eq}/\ell\right)}{\left(\ell/d\right)\sin\left(\pi d/\ell\right)} \tag{76}$$

where $11d$ has been taken as ℓ_{eq} in the final expression. At resonance, this becomes

$$A_1 \approx I_{s0}Q_1\left(\eta_0/Z_0\right)\frac{\alpha_m\left\{\ell_{eq}/\ell-\frac{\sin(\pi\ell_{eq}/\ell)}{(\ell/d)\sin(\pi d/\ell)}\right\}-\alpha_e\left\{\ell_{eq}/\ell+\frac{\sin(\pi\ell_{eq}/\ell)}{(\ell/d)\sin(\pi d/\ell)}\right\}}{\pi^2 c_i c_e d}f_{4E} \tag{77}$$

and because $\sin\left(\pi d/\ell\right) \approx \pi d/\ell$ this result is expected to nearly agree with the previous continuous approximation (67). In fact for $\ell \approx 26$ in. and $d \approx 2$ in ($\sin\left(\pi d/\ell\right)$ and $\pi d/\ell$ differ by less than 1%) and a quality factor of 177.3 (calculated in the previous section), (77) yields $A_1/I_{s0} \approx -20.9$ dB and is in agreement with (68), and for the slotted tube $A_1/I_{s0} \approx -14.4$ dB in agreement with (69).

3.4 MODEL COMPARISONS AND EXPERIMENTAL RESULTS

In this section shielding effectiveness calculations for the two standard calibration tubes are compared to the measured results obtained using the cable tester arrangement shown in Fig. 1. Because we need more information about the load values associated with the current probes at the ends of the tester, the first subsection discusses some work done to improve our understanding of these loads as a function of frequency, particularly in the vicinity of the resonance of the device. The comparisons are then done using assumed loads that are consistent with this load characterization.

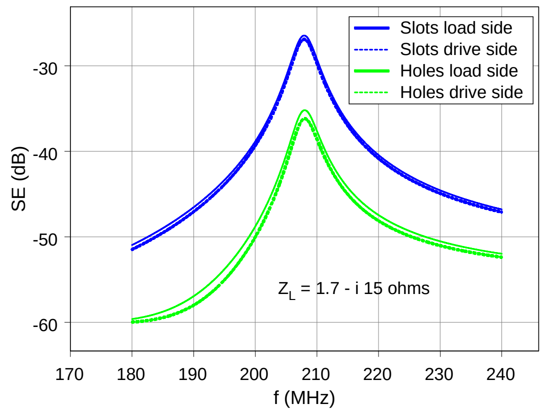

Figure 7. A comparison of the two calibration tube responses with loads of $Z_L = 1.7 - i15$ ohms.

3.5 Loads And Adaptors

The current probes at the ends of the cable tester represent $Z_L \to 0.5$ ohm loads at low frequencies, as stated above. Near the resonance of the tester (with the calibration tubes) at $f \approx 208$ MHz it was found that the loads exhibit increasing losses as well as reactive effects; an assumed load value $Z_L \approx 1.7 - i15$ produced approximately the correct quality factor as well as resonant position. Results near the resonance with this fit for both the slotted and circular hole calibration tubes are shown in Figure 7.

To get a better understanding of these load values several experiments were performed. An original adaptor from a type N connector to the current probe, shown in Figures 8 and 9, was used to connect the current probe to the network analyzer and perform reflection measurements as shown in Figure 11. These yielded a range of values depending on which current probe was examined, $Z_L \approx 3 - i53$ ohms to $3.7 - i54.7$ ohms. It was realized that the large capacitance to ground associated with this original adaptor design was responsible for the difference in value being measured versus the values used to fit the cable tester model to the response data.

The adaptor was redesigned as shown in Figures 8 and 10 to reduce this capacitance. The new measurements of the current probe loads were $Z_L \approx 1.58 - i31.6$ ohms to $1.51 - i32.0$ ohms. The real part is now in the ballpark of what was required in the fit. We see that the reactive part has also been reduced but it is difficult to measure this accurately. It is interesting that, even for the moderate frequencies ($f \approx 200$ MHz) being considered in this experiment, it is a challenge to obtain accurate values for these nonstandard loads. This represents an analog of what we face in characterizing the high frequency behavior of audio frequency components at the ends of multconductor cables.

These new adaptors are also used for testing more standard cables in the cable tester as shown in Figure 12, where dielectric weights are used to secure the cable to the ground plane and paper shims are used to provide a known and constant spacing (referred to as h in the preceding analysis) between the cable and the ground plane.

3.5.1 Calibration Tube Shielding Effectiveness

The experimental shielding effectiveness of the circular-hole calibration tube is shown in Figure 13. The

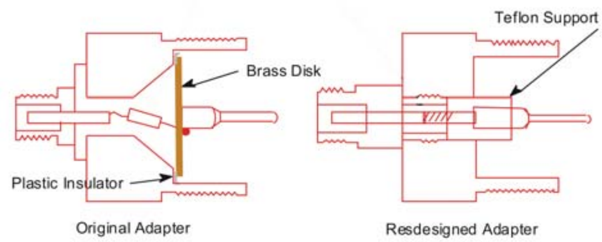

Figure 8. Drawing of original and redesigned adaptors.

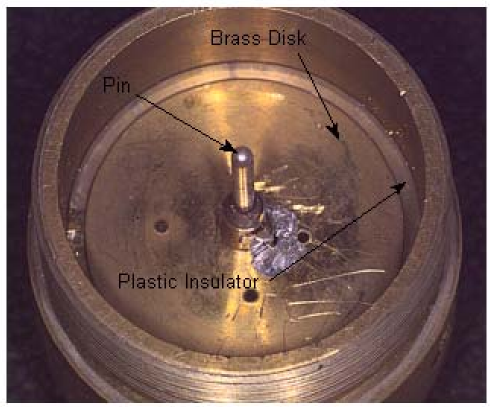

Figure 9. Original current probe to cable adaptors.

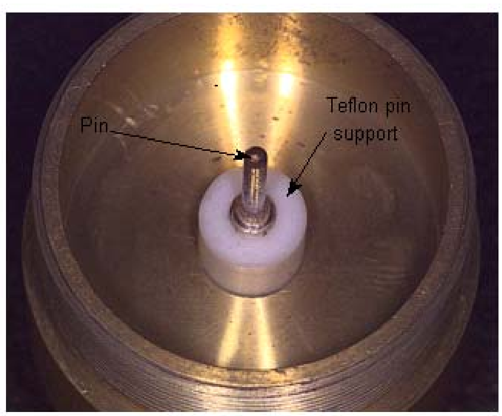

Figure 10. Redesigned current probe to cable adaptors.

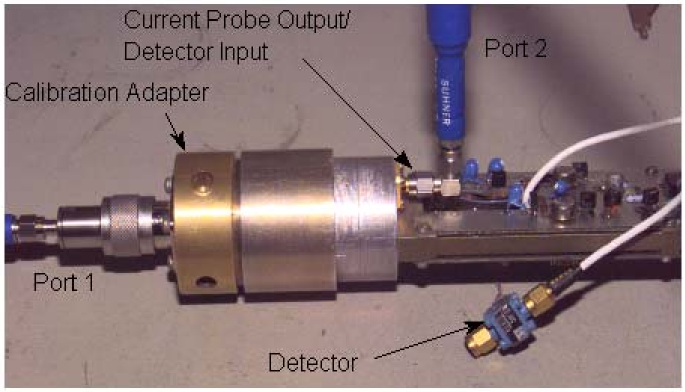

Figure 11. The measurement system used to sample the interior transmission line current in the cable tester setup.

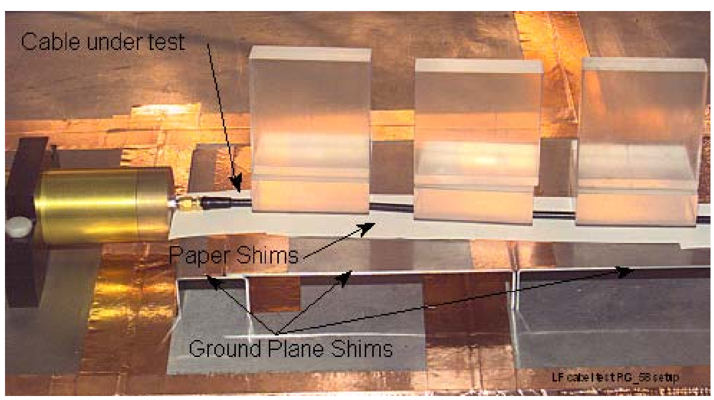

Figure 12. The cable tester setup with adaptor for measuring the shielding effectiveness of a flexible coaxial cable.

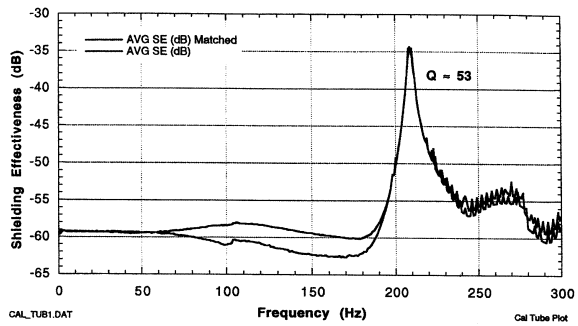

Figure 13. Experimental shielding effectiveness from the circular hole calibration tube. The experimental quality factor is noted on the graph.

experimental quality factor is also noted on the graph. Figure 14 shows the predicted shielding effectiveness from (52) for both the low frequency load values and the fit to the resonant behavior of the current probes. The 0.5 ohm load values mimic the low frequency behavior, but the loads exhibit more loss at the higher frequencies.

Figure 15 shows a comparison of experimental results and predicted results for the slotted calibration tube. The experimental results are the black curves and the model results are the grey curves from (52).

4 SUMMARY

In this report two standard calibration cables were examined from both an analytic model and experimental point of view. The analytic model is based on a transmission-line approach and is used to evaluate the current induced on the inner conductor of the cable (relative to the exterior current driven on the outer shield of the cable) due to penetrations of the electromagnetic fields through the shield apertures. The transmission line representation for the cable contains distributed voltage and current sources used to model the leakage of magnetic and electric fields through the shield apertures (for this report, periodic circular holes or rectangular slots), as well as distributed inductance and capacitance parameters which capture the energy storage (and distributed resistance to represent absorption, if applicable) associated with the physical characteristics of the cable. The source terms in the transmission line model are given in terms of the magnetic and electric dipole moments induced in the shield apertures and are a function of the shield geometry.

A general solution for the shielding effectiveness of the calibration standards are provided and, for convenience, approximate formulas in the limiting cases of low frequency and at resonance are also given. These have been shown to yield good agreement with the more rigorous shielding effectiveness derivation and hence can be used to quickly assess (or perhaps bound) the shielding performance of the cable.

To complement and compare with the analytic formulation, shielding effectiveness measurements using a cable tester setup were also performed. Two types of calibration tubes were constructed, one having circular hole penetrations and the other having narrow slot penetrations. The slotted calibration tube was designed to exhibit the same low frequency magnetic penetration but no significant electric penetration. In comparing the analytic and experimental results, it became clear that the characterization of the load impedance on the interior conductor is important in accurately modeling the shielding effectiveness both at very low frequencies (where the end loads eventually dominate over the inductance of the coaxial tube) and at resonance (where the real part largely determines the peak level and the reactive part influences the

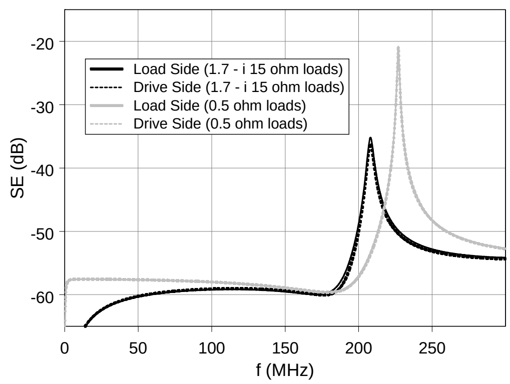

Figure 14. Predicted results for the circular hole calibration tube for two load values associated with the current probes.

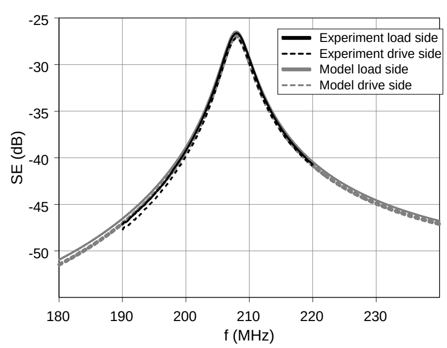

Figure 15. The calculated (grey curves) and measured (black curves) shielding effectiveness for the slotted-aperture calibration standard containing an interior load impedance equal to $Z_L \approx 1.7 - i15$ ohms are shown.

resonant position). Accurate determination of these current probe load values near the tube resonance posed a challenge, despite the moderate frequency of operation considered. The slotted tube has considerably larger resonant penetration than the circular tube due to cancellation of the magnetic and electric parts in the circular hole apertures.

The analysis of the calibration tube setup was done to improve our understanding the performance of the tester in order to properly interpret its response with actual shielded multiconductor cables. In addition, this setup forms an instructive arrangement since issues, such as cancellation of components of the penetration as well as end load component characterizations (in this case the current probes), arising in the modeling are similar to those arising with actual cables, but in a more controlled and repeatable geometry.

5 REFERENCES

[1] J.S. Hofstra and L.O. Hoeft, "Measurement of Surface Transfer Impedance of Multi-Wire Cables, Connectors, and Cable Assemblies," Record of the IEEE International Symposium on EMC, 1992.

[2] M. E. Morris, B. Stiefeld, and M. Valencia, "Calibration Standard Analysis and Fabrication for RF Cable Tester - Test System 970 (CP-SE 1260)," Sandia National Laboratories internal memorandum, to J. C. Bushnell, September 29, 1981.

[3] K. C. Chen, J. E. Solberg, R. H. Bonn, T. E. Koontz, S. W. Holmes, L. K. Warne and M. E. Morris, "Braided Shield and Cable Shielding Effectiveness Test," Sandia National Laboratories internal memorandum, 1986.

[4] F. M. Tesche, M. V. Ianoz, and T. Karlsson, EMC Analysis Methods and Computational Models, New York: John Wiley & Sons, Inc., Chapter 9, 1997.

[5] R. W. Latham, "Small Holes in Cable Shields," AFWL Interaction Note 118, September 1972.

[6] K. S. H. Lee, *EMP Interaction: Principles, Techniques, and Reference Data*, New York: Hemisphere Pub., 1986, pp. 186-188, 436-441, 518-522, 578-593.

[7] N. A. McDonald, "Electric and Magnetic Coupling Through Small Apertures In Shield Walls of Any Thickness," IEEE, Trans. on Microwave Techniques, MTT-20, pp. 689-695, 1972.

[8] R. L. Gluckstern and J. A. Diamond, "Penetration of Fields Through a Circular Hole in a Wall of Finite Thickness," IEEE Transactions on Microwave Theory and Techniques, Vol. 39, No. 2, February 1991. (Note that there is an error in equation (59), the constant should be -0.176 rather than -0.716. See the table in this paper or see "Magnetic field leakage into a semi-infinite pipe," R. W. Latham and K. S. H. Lee, Canadian J. of Physics, Vol. 46, pp. 1455-1462, 1968.)

[9] L. K. Warne and K. C. Chen, "A Simple Transmission Line Model for Narrow Slot Apertures Having Depth and Losses," IEEE Transactions on Electromagnetic Compatibility, Vol., 34, No. 3, August 1992.

[10] L. K. Warne, T. E. Koontz, and K. C. Chen, "Equivalent Polarizabilities of apertures with Depth," AFWL Interaction Note 474, March 1989.

[11] S. Ramo, J. R. Whinnery, and T. Van Duzer, *Fields and Waves in Communication Electronics*, New York: John Wiley & Sons, Inc., pp. 31-33, 288-289, 1965.

Intentionally Left Blank

DISTRIBUTION

Number	Mail Stop	Name	Dept.
1(electronic)	MS0405	K. O. Merewether	0434
1 (electronic)	MS0447	M. E. Morris	2111
1 (electronic)	MS0492	K. C. Chen	0411
2	MS1152	L. I. Basilio	1352
1 (electronic)	MS1152	R. E. Jorgenson	1352
2	MS1152	W. L. Langston	1352
3	MS1152	L. K. Warne	1352
1 (electronic)	MS1152	H. G. Hudson	1353
1 (electronic)	MS1152	M. Jursich	1353
1 (electronic)	MS1152	R. A. Salazar	1353
1 (electronic)	MS1168	B. V. Oliver	1352
1 (electronic)	MS0899	RIM - Reports Management	9532

Intentionally Left Blank

Sandia National Laboratories